



Article

Li₄SiO₄-Based Heat Carrier Derived from Different Silica Sources for Thermochemical Energy Storage

Xicheng Wang ^{1,2}, Wentao Xia ^{1,2}, Wenlong Xu ^{1,2}, Zengqiao Chen ^{1,3,*}, Xiaohan Ren ^{1,2,*}  and Yuandong Yang ^{1,2,*} ¹ Institute of Thermal Science and Technology, Shandong University, Jinan 250061, China; wangxc0108@163.com (X.W.); xiawt998@163.com (W.X.); xuwenlong@sdu.edu.cn (W.X.)² Institute for Advanced Science and Technology, Shandong University, Jinan 250061, China³ School of Energy and Power Engineering, Shandong University, Jinan 250061, China

* Correspondence: czq@sdu.edu.cn (Z.C.); renxh@sdu.edu.cn (X.R.); yyd@sdu.edu.cn (Y.Y.)

Abstract: Thermochemical energy storage (TCES) is one of the key technologies facilitating the integration of renewable energy sources and mitigating the climate crisis. Recently, Li₄SiO₄ has been reported to be a promising heat carrier material for TCES applications, owing to its moderate operation temperature and stability. During the synthetic processes, the properties of the Si source used directly influence the performance of derived Li₄SiO₄ materials; however, the internal relations and effects are not yet clear. Hence, in this work, six kinds of SiO₂ sources with different phases, morphology, particle size, and surface area were selected to synthesize a Li₄SiO₄-based TCES heat carrier. The physicochemical properties of the SiO₂ and the corresponding derived Li₄SiO₄ were characterized, and the comprehensive performance (e.g., heat storage/releasing capacity, rate, and cyclic stability) of the Li₄SiO₄ samples was systematically tested. It was found that the silica microspheres (SPs), which possess an amorphous phase, uniform micro-scale structure, and small particle size, could generate Li₄SiO₄ TCES materials with a highest initial capacity of 777.7 kJ/kg at 720 °C/900 °C under pure CO₂. As a result, the SP-L showed an excellent cumulative heat storage amount of 5.84 MJ/kg within 10 heat-releasing/storage cycles, which was nearly 1.5 times greater than the value of Li₄SiO₄ derived from commonly used silicon dioxide. Furthermore, the effects of the utilized Si source on the performance of as-prepared Li₄SiO₄ and corresponding mechanisms were discussed, which offers guidance for the future selection of Si sources to produce high-performance Li₄SiO₄-based TCES heat carriers.

Keywords: Li₄SiO₄; silicon source; CO₂ capture; thermochemical energy storage**Citation:** Wang, X.; Xia, W.; Xu, W.; Chen, Z.; Ren, X.; Yang, Y.Li₄SiO₄-Based Heat Carrier Derived from Different Silica Sources for Thermochemical Energy Storage.*Energies* **2024**, *17*, 2180. <https://doi.org/10.3390/en17092180>

Academic Editor: K. T. Chau

Received: 3 April 2024

Revised: 27 April 2024

Accepted: 29 April 2024

Published: 2 May 2024



Copyright: © 2024 by the authors. Licensee MDPI, Basel, Switzerland. This article is an open access article distributed under the terms and conditions of the Creative Commons Attribution (CC BY) license (<https://creativecommons.org/licenses/by/4.0/>).

1. Introduction

In recent years, in order to slash fossil fuel consumption and mitigate the climate change crisis, renewable energy technologies have been significantly developed, and their proportion in energy structures is continuously rising [1–3]. Nevertheless, the inherent stochasticity, volatility, and intermittency of renewable energy sources, such as solar and wind energy, pose challenges to the reliability, stability, and security of modern power systems. Energy storage technology (EST) has been considered as one of the most major solutions to overcome these disadvantages and determine the flexibility of electricity [4,5].

Based on their different working principles, the existing energy storage technologies can be categorized as mechanical energy storage (e.g., pumped hydro storage, compressed air energy storage, and flywheel storage), electrochemical energy storage (e.g., lithium-ion battery, sodium-ion battery, and Ni-Cd battery), electrical energy storage (e.g., supercapacitor and superconducting magnet), chemical energy storage (e.g., fuel cell and power to X), and thermal energy storage [6,7]. Among them, thermal energy storage (TES) has gained increasing attention due to its high energy density and potential for large-scale and long-duration energy storage applications [8]. It can be further divided into sensible

thermal energy storage (STES), latent thermal energy storage (LTES), and thermochemical energy storage (TCES), depending on the heat storage mechanisms and utilized medium. Currently, STESs using thermal oil and LTESs using phase change materials (PCMs) like molten salts have been commercially applied in concentrated solar power (CSP) plants, enabling the efficient storage of solar heat for cross-time utilization [9,10]. However, as the CSP technology rapidly upgrades, the next generation large-scale solar tower power plant was predicted to achieve higher temperatures surpassing 700 °C [11], at which the TCES shows outstanding advantages due to the excellent thermostability and volumetric energy storage density (commonly > 500 kWh/m³) of the TCES heat carrier materials [12,13].

Up to now, a series of materials have been reported to act as heat carriers for TCES applications, including hydroxides (e.g., CaO/Ca(OH)₂) [14,15], oxides (e.g., Fe₂O₃/Fe₃O₄) [16,17], carbonates (e.g., CaO/CaCO₃) [18–20], and sulfates (e.g., MgO/MgSO₄) [21]. Among them, the Li₄SiO₄-based heat carrier, which operates at the 600–900 °C medium temperature region and possesses a theoretical storage density of 784.3 kJ/kg, has been considered a potential candidate [22,23]. Although using Li₄SiO₄ materials to act as a CO₂ adsorber for carbon capture and storage (CCS) has been widely investigated in recent years, its research on TCES applications is currently limited [24,25]. Figure 1 illustrates the basic flow of a Li₄SiO₄-CO₂ TCES system based on reversible carbonation–decarbonation reactions. As shown, during the heat storage process, the Li₂SiO₃ reacts endothermically with Li₂CO₃ to generate Li₄SiO₄ and CO₂ in the left heat storage reactor. When thermal energy is demanded, the Li₄SiO₄ and CO₂ are transported to the heat-releasing reactor to regenerate Li₂SiO₃ and Li₂CO₃ by releasing heat, thus forming the cyclic heat storage–releasing processes.

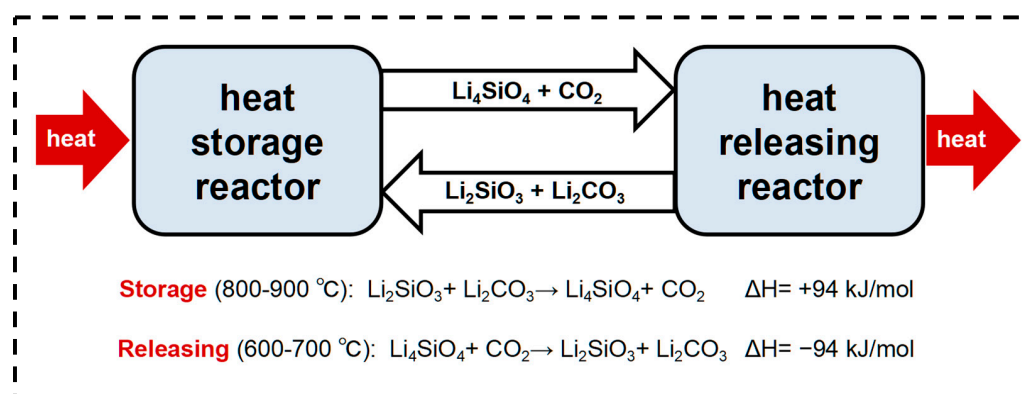


Figure 1. Schematic illustration of a Li₄SiO₄-CO₂ TCES system.

The comprehensive performance of a Li₄SiO₄ heat carrier, mainly including the heat storage/releasing capacity and the cyclic stability, directly determines the operation efficiency and operation life of Li₄SiO₄-CO₂ TCES systems [26,27]. Hence, various approaches have been reported to improve the performance of Li₄SiO₄. Doping is a convenient and effective way, that is, mixing Li₄SiO₄ with other chemicals to change its reaction properties. For example, doping K₂CO₃ in Li₄SiO₄ could turn the Li₂CO₃ solid shell to eutectic Li₂CO₃-K₂CO₃ during Li₄SiO₄-CO₂ reactions, thus reducing the diffusion resistance of CO₂ molecules and making the reaction more sufficient [28,29]. The introduction of heteroatoms in Li₄SiO₄, like Fe-doping or Ce-addition, could form lattice defects or inert skeletons, thus increasing both the reaction capacity and the cyclic stability of the Li₄SiO₄ heat carrier significantly [30,31]. The optimization of synthetic processes could also improve the performance of the obtained Li₄SiO₄, especially the selection of raw materials. Traditionally, the Li₄SiO₄ heat carrier was synthesized using Li₂CO₃ and SiO₂ as the Li source and Si source, and the as-synthesized sample shows a relatively poor heat storage capacity of 470–600 kJ/kg within 20 cycles, which only reaches 60–77% of the theoretical value of Li₄SiO₄ [32]. Recent research has reported that the utilization of an organic lithium precursor to replace Li₂CO₃ could effectively optimize the structure and morphology of as-prepared Li₄SiO₄,

thus increasing its heat storage capacity to more than 700 kJ/kg [29,30,33]. Although the effect of the Li source has been revealed, it should be noted that the Li sources will turn to liquid during the high-temperature synthesis of Li_4SiO_4 , and the Si source is the only solid phase in this process [34,35]. Hence, it could be predicted that the properties of the Si sources used are strongly related to the properties and performance of the obtained Li_4SiO_4 heat carrier. However, the effect of different Si sources on the TCES performance of as-prepared Li_4SiO_4 and corresponding mechanisms are still unreported, which is essential to investigate and clarify.

For these reasons, in this work, six kinds of SiO_2 with different phases, morphology, particle size, and surface area were employed to synthesize Li_4SiO_4 -based heat carrier materials. The physicochemical properties, as well as the comprehensive performance of the SiO_2 and corresponding derived Li_4SiO_4 samples, were systematically investigated and compared. The effect of the Si source utilized on the performance of as-prepared Li_4SiO_4 and corresponding mechanisms were determined in depth, which could provide guidance for the future selection of a Si source to produce high-performance Li_4SiO_4 TCES materials.

2. Experimental Section

2.1. Synthesis of Li_4SiO_4 -Based Materials

For the preparation of Li_4SiO_4 , Li_2CO_3 (AR, Sinopharm) served as the Li source, and six kinds of different reagents were selected as the Si source. These reagents, including silicon dioxide (abbreviated to S, AR, Sinopharm), silica microspheres (abbreviated to SP, AR, Qinghe Andi), silica sol (abbreviated to SS, 30 wt.% SiO_2 in water, industrial grade, Guangzhou Suixin), fumed silica (abbreviated to FS, AR, Aladdin), SBA-15 (abbreviated to SBA, Aladdin), and quartz sand (abbreviated to QS, AR, Sinopharm), were all mainly composed of SiO_2 .

The synthetic processes of Li_4SiO_4 were as follows: (I) the selected Si sources were mixed with Li_2CO_3 and deionized water by controlling the molecule ratio, which equaled Si–Li of 1:4.2, in which the excessive amount of lithium was to compensate for the sublimation loss during high-temperature calcination; (II) then, the mixed liquids were continuously stirred and heated at 80 °C in an oil bath until complete evaporation; (III) the evaporated mixtures were subsequently calcined at 800 °C for 4 h in a muffle oven with a heating rate of 10 °C/min; (IV) after calcination, the obtained Li_4SiO_4 blocks were ground and sieved to <200 μm . The final produced Li_4SiO_4 powder was named M-L, in which the M means the abbreviation of the used Si source. For example, FS-L means the Li_4SiO_4 materials synthesized from fumed silica.

2.2. Characterizations and Performance Tests

Phase compositions of as-prepared Li_4SiO_4 -based materials were determined by an X-ray diffractometer (XRD, Empyrean, PANalytical B. V.) using $\text{CuK}\alpha$ radiation ($\lambda = 1.54 \text{ nm}$) with 2θ ranging from 15° to 70°. The N_2 absorption–adsorption isotherms of the materials were measured at 77 K using a surface area analyzer (3Flex, Micromeritics), and corresponding specific surface areas were calculated according to the Brunauer–Emmett–Teller (BET) method. The morphology of the samples was observed with a field-emission scanning electron microscope (SEM, Nova NanoSEM 450, FEI) with an extra high tension (EHT) of 20 kV. Particle size distributions (PSDs) of samples were detected by a laser particle size analyzer (LPSA, Mastermin, Malvern) using absolute alcohol as measuring media.

The CO_2 capture performance and the corresponding thermochemical energy storage capacity of Li_4SiO_4 -based materials were systematically evaluated with a thermogravimetric analyzer (TGA, STA449F3, Netzsch, Germany). First, dynamic heating-up tests were carried out to find the temperature window of CO_2 adsorption and desorption reactions, in which the tested samples were continuously heated from room temperature to 1000 °C at a speed of 10 °C/min under a 100% CO_2 atmosphere. Then, the isothermal adsorption test was used to determine the optimal heat-releasing temperature of Li_4SiO_4 . The samples were heated to 900 °C under pure N_2 for complete regeneration and then

maintained at selected temperatures (680, 700, and 720 °C) for 30 min under a 100% CO₂ adsorption atmosphere. After that, the optimal temperature of CO₂ desorption (also the heat storage reaction) was determined by a non-isothermal desorption test, in which the fully adsorbed Li₄SiO₄ was heated to selected desorption temperatures (850 and 900 °C) for 20 min under 100% CO₂. Finally, a cyclic ad-desorption test was performed to estimate the comprehensive energy storage/releasing performance of Li₄SiO₄ TCES materials during 10 CO₂ adsorption–desorption cycles. In each cycle, the tested samples react with CO₂ at the optimal adsorption temperature for 20 min and then desorb at the selected desorption temperature for 20 min under a pure CO₂ atmosphere. The results of the above TG tests were quantitatively analyzed to calculate the adsorption capacity, regeneration ratio, heat storage capacity, and cumulative storage capacity of the Li₄SiO₄ materials, and their detailed definitions and calculation formulas have been described in our previous work [30,36].

3. Results and Discussion

First of all, XRD patterns of the Si sources and the corresponding derived Li₄SiO₄ samples were scanned to identify the phase changes during the synthetic process. As seen in Figure 2a, there exists significant differences among these Si sources. The quartz and silicon dioxide were composed of the SiO₂ phase (JCPDS 29-0085), while no obvious diffraction peak could be found in other samples. That indicates that the SP, SS, FS, and SBA are mainly composed of amorphous silica, which is reported to be preferable for the performance of the derived Li₄SiO₄ [37]. The phase compositions of as-prepared samples were further determined in Figure 2b. All samples were mainly composed of the Li₄SiO₄ phase (JCPDS 20-0637), ensuring the feasibility of the synthesis methods and synthesis conditions utilized in this work. However, a small fraction of impurities, including Li₂SiO₃ and Li₂CO₃, could be found in some patterns, which may affect their performance during Li₄SiO₄-CO₂ reactions. Moreover, in comparison with S-L and QS-L, the other four samples, especially the SP-L, showed a low-intensity pattern. According to Scherrer's equation, the intensity decrease in the peak leads to a lower value of the full width at half maxima (FWHM) and a smaller Li₄SiO₄ crystal size, which is reported to be beneficial for enhancing both the chemisorption and the diffusion during Li₄SiO₄-CO₂ reactions [38].

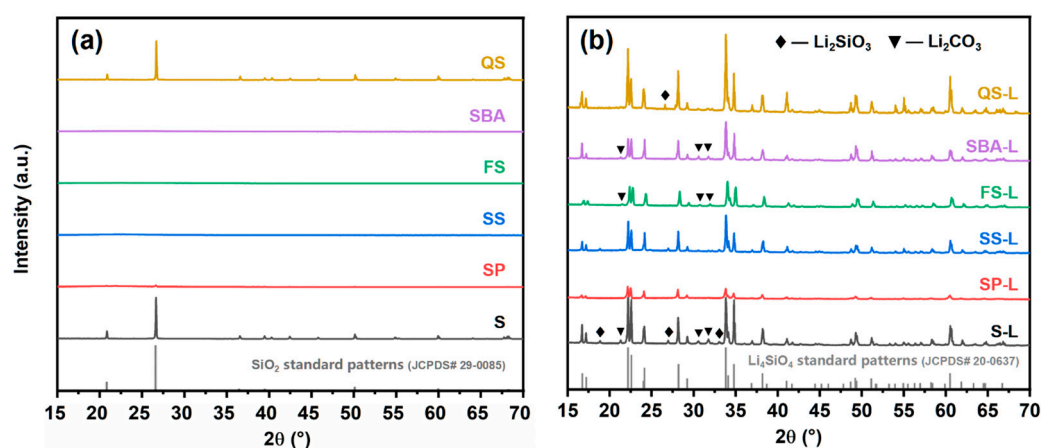


Figure 2. XRD patterns of (a) different Si sources and (b) corresponding derived Li₄SiO₄ samples.

The morphology of the Si sources and the corresponding derived Li₄SiO₄ samples was observed by SEM, and the images are provided in Figure 3. Among these Si sources, the S and QS exhibited a similar bulked appearance with a large size of more than 50 µm, while the SP and SS were, respectively composed of regular spherical and fragmental particles with a size of 1–20 µm. The FS and SBA showed a much smaller morphology consisting of nano-sized SiO₂ structures, as seen in the enlarged 20,000× magnification images. After being calcined at 800 °C for 4 h, all as-prepared samples showed an agglomerated mor-

phology with a larger size, which could be attributed to the particle sintering occurring under high temperatures. Especially, the nanostructure of FS and SBA totally disappeared, and the synthesized FS-L and SBA-L exhibited a highly-sintered and non-porous bulked appearance similar to others.

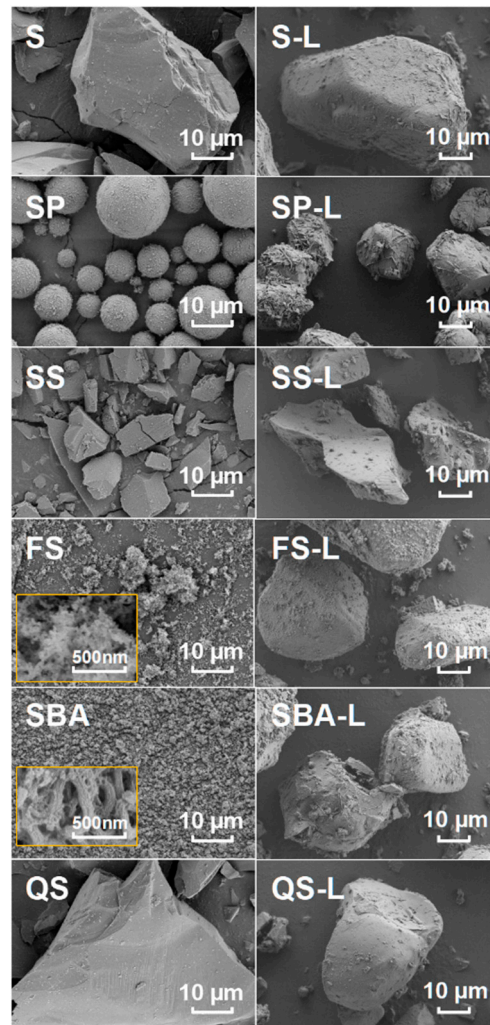


Figure 3. SEM images of different Si sources and corresponding derived Li_4SiO_4 samples.

A laser particle size analyzer was then used to evaluate the PSDs and the average diameter of the Si sources and corresponding Li_4SiO_4 samples, as shown in Figure 4, where the parameter D_{v50} denotes the median diameter of the tested sample. The value of D_{v50} represents the particle size below which 50% of the particles, by volume, are distributed. Except for QS, all Si sources possessed an average diameter as low as 13–49 μm ; however, the D_{v50} of all samples dramatically increased to 64–105 μm after synthesis. This particle size increment trend, which should be attributed to the particle sintering during the high-temperature calcination process, is basically consistent with the findings in SEM observations. Moreover, it was found that, although the particle size distributions of the Si sources were quite different and disordered, the curves of the synthesized Li_4SiO_4 were relatively similar after being calcined, ground, and sieved.

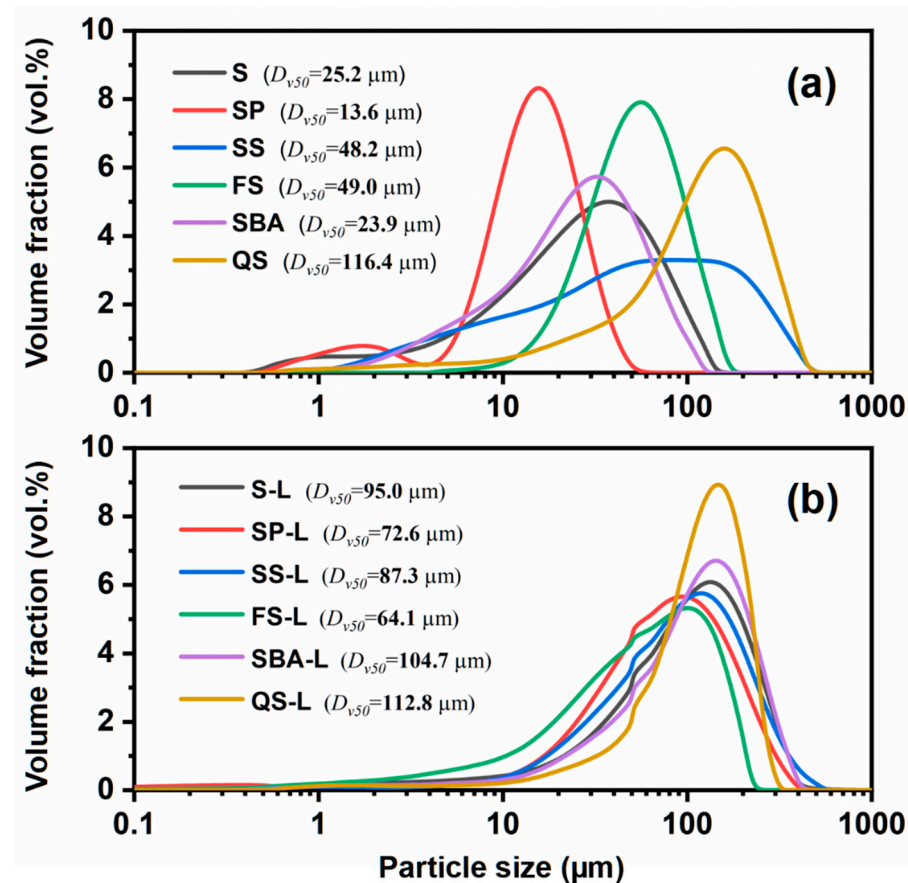


Figure 4. PSDs and average particle size of (a) Si sources and (b) as-synthesized samples.

Table 1 lists the BET-specific surface area of Si sources and as-synthesized samples measured by N_2 adsorption–desorption. As seen, the values of these Si sources, ranging from 0.1 to nearly 1000, show remarkable differences. The poor surface area of S and QS was mainly caused by their large bulk appearance, as found in former tests. In comparison, the SS, FS, and SBA, which had improved morphology and smaller particle sizes, exhibited a greater surface area higher than 200. It should be noted that although the SP also possessed a smaller particle size, its smooth, non-porous, and regular spherical appearance led to a limited BET value of only $\sim 2 \text{ m}^2/\text{g}$. Then, after the synthetic process, all as-prepared Li_4SiO_4 samples were highly sintered due to high-temperature calcination, and their BET surface area sharply decreased to $< 2 \text{ m}^2/\text{g}$. The values of SP-L, SS-L, FS-L, and SBA-L were nearly 2 times higher than those of S-L and QS-L, which are in accordance with the results of SEM and LPSA tests.

Table 1. BET specific surface area of Si sources and as-synthesized samples.

Si Sources	Surface Area (m^2/g)	Li_4SiO_4 Samples	Surface Area (m^2/g)
S	0.303	S-L	0.914
SP	2.167	SP-L	1.825
SS	237.802	SS-L	1.788
FS	208.058	FS-L	1.883
SBA	879.750	SBA-L	1.682
QS	0.262	QS-L	0.810

The comprehensive CO_2 capture performance, as well as the heat storage capacity of as-prepared Li_4SiO_4 -based materials, were evaluated by a series of TG tests. The dynamic heating-up test was first performed for the preliminary selection of the temperature ranges of the Li_4SiO_4 - CO_2 adsorption and desorption reactions. The tested samples were heated

from room temperature to 1000 °C by 10 °C/min in 100% CO₂, and their weight change curves during the test are shown in Figure 5. As seen, the weight of all samples started to show a growing trend at temperatures higher than 500 °C, and the weight gain became more rapid as the temperature increased. This should be attributed to the CO₂ adsorption of Li₄SiO₄, in which the Li₄SiO₄ begins to react with CO₂ at ~500 °C, and this reaction could be enhanced at higher temperatures due to the acceleration of gas molecules' thermal motion. When the temperature increased to 700–720 °C, the weight change curves reached the highest values, corresponding to the achievement of an equilibrium state between CO₂ adsorption and CO₂ desorption reactions. In addition, it was also found that the SP-L, SBA-L, and SS-L exhibited a maximum weight gain exceeding 30%, revealing that their performance in CO₂ capture and heat storage should be considerable. Then, as the temperature continued to increase, the desorption reaction took the dominant position, and all curves began to decrease sharply. At 850–900 °C, the samples achieved complete desorption, and the weight curves returned to ~100%. Hence, the temperature windows of CO₂ adsorption and CO₂ desorption reactions are, respectively selected as 680–720 °C and 850–900 °C in the following tests.

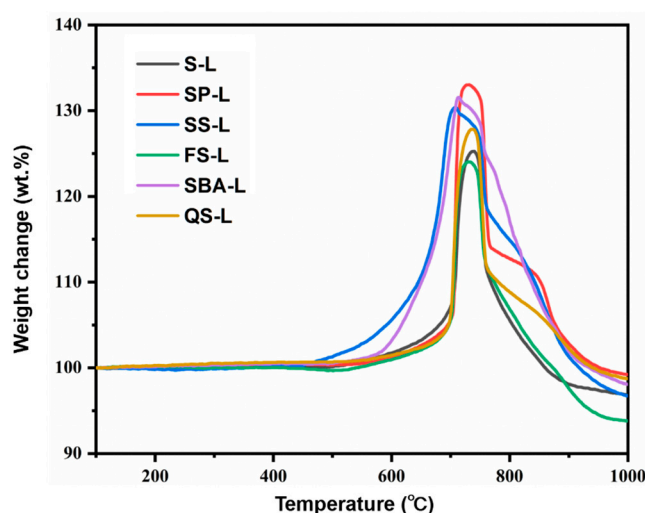


Figure 5. Dynamic heating-up adsorption–desorption curves of as-prepared Li₄SiO₄ samples.

An isothermal CO₂ adsorption test was then carried out to select the optimal adsorption temperature and screen the adsorption performance of the different Si source-derived Li₄SiO₄. The samples were heated at 680 °C, 700 °C, and 720 °C under 100% CO₂ for 30 min and the obtained curves are shown in Figure 6. Except for SS-L and SBA-L, the CO₂ adsorption capacity of other Li₄SiO₄ materials was as low as <0.1 g/g at 680 °C, even after 30 min adsorption, indicating that this temperature is not suitable for the reactions. The differences should be attributed to the diverse reaction temperature window of as-prepared Li₄SiO₄ samples. As seen in Figure 5, the curves of SS-L and SBA-L show a wider temperature window, resulting in its high performance during all isothermal adsorption tests at 680 °C, 700 °C, or 720 °C. In comparison, the other Li₄SiO₄ samples show a slow reaction slope at 680 °C, corresponding to their poor isothermal adsorption capacity, as observed in Figure 6. As the temperature increased, the adsorption performance of the samples was greatly increased, and all of them exhibited a capacity exceeding 0.3 g/g at 720 °C. Especially, SP-L and SS-L showed the greatest adsorption capacity and fastest adsorption rate of >0.335 g/g within only 5 min, which should be attributed to their superior physicochemical properties, such as purity, morphology, and so on, as detected in previous characterizations. As a consequence, SP-L and SS-L were screened out for the following cyclic tests, and their optimal adsorption temperature was selected as 720 °C.

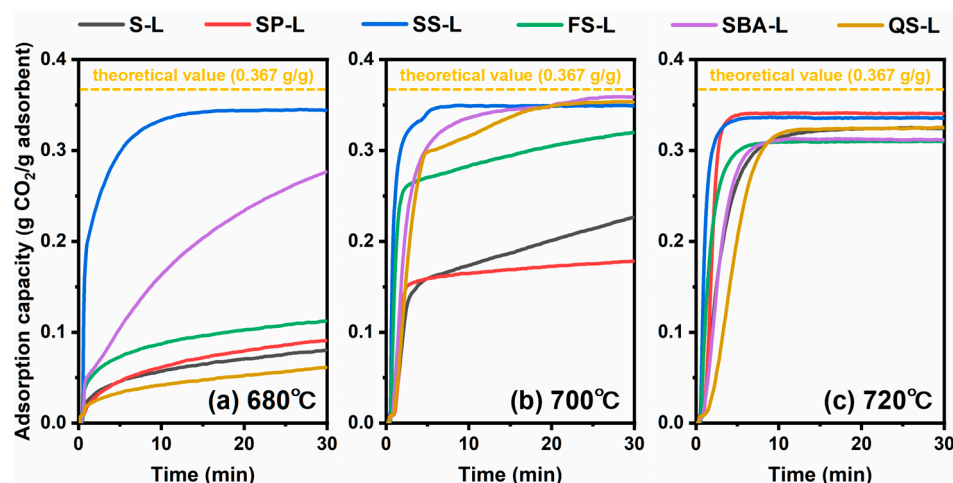


Figure 6. Isothermal CO₂ adsorption curves of as-prepared Li₄SiO₄ samples at (a) 680 °C, (b) 700 °C, and (c) 720 °C.

The desorption performance and the optimal desorption temperature of the samples were investigated by non-isothermal desorption tests. As illustrated in Figure 7, the fully adsorbed samples were heated from 720 °C to a selected desorption temperature (850 °C and 900 °C) at a rate of 20 °C/min under a 100% CO₂ atmosphere and then maintained at this temperature until the desorption time reached 20 min. After a 20 min reaction, the regeneration ratio of the samples reached 80–95% under the 850 °C test condition, and it was greatly increased to >95% when the desorption temperature was 900 °C. Hence, the desorption conditions in the following cyclic test were selected as 900 °C for 20 min to ensure the full desorption of Li₄SiO₄. Moreover, it should be noted that there were no remarkable differences among the desorption curves of these samples at 900 °C, revealing the change in Si sources has a limited effect on the desorption performance of Li₄SiO₄ adsorbents.

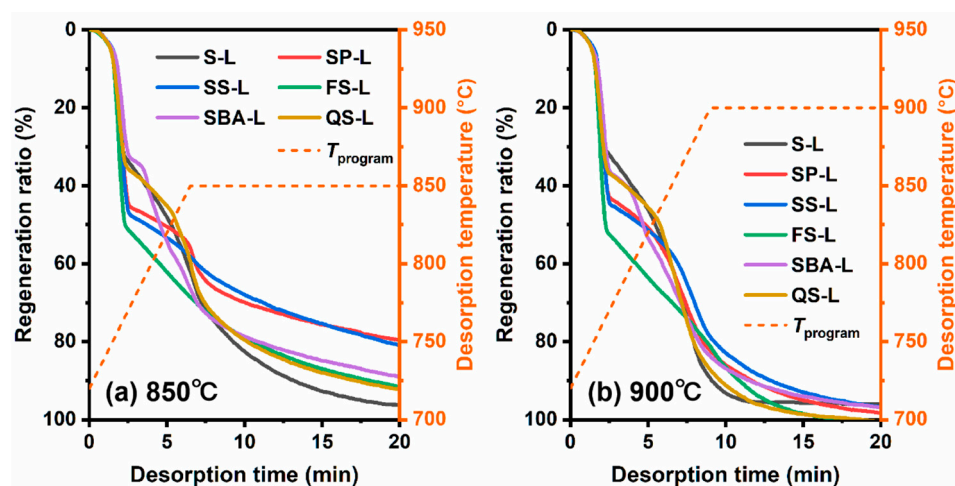


Figure 7. Non-isothermal CO₂ desorption curves of as-prepared Li₄SiO₄ samples at (a) 850 °C and (b) 900 °C.

The comprehensive capture performance and heat storage performance of Li₄SiO₄ samples were determined by a cyclic CO₂ ad-desorption test. Except for the selected SS-L and SP-L, the S-L, which was derived from commonly used SiO₂, was also picked for comparison. In each cycle, the reactions proceeded under a flowing pure CO₂ atmosphere, and the tested sample first adsorbed CO₂ at 720 °C for 20 min and then turned to desorption at 900 °C for 20 min. The weight change curves within 10 cycles were recorded, and the corresponding ad/desorption capacities were calculated, as shown in Figure 8a. All samples exhibited an excellent capacity of 0.32–0.36 g/g at the initial cycle, which is in

accordance with the results of the isothermal test. Nevertheless, the maximum values decreased as the cycle number increased. The S-L suffered a sharp capacity decrement at the beginning of four cycles and was finally maintained at ~ 0.18 g/g, which was only half as much of the theoretical capacity of Li_4SiO_4 . In comparison, the curves of SP-L and SS-L showed a slow and uniform descent and possessed a capacity of 0.23–0.25 g/g at the 10th cycle.

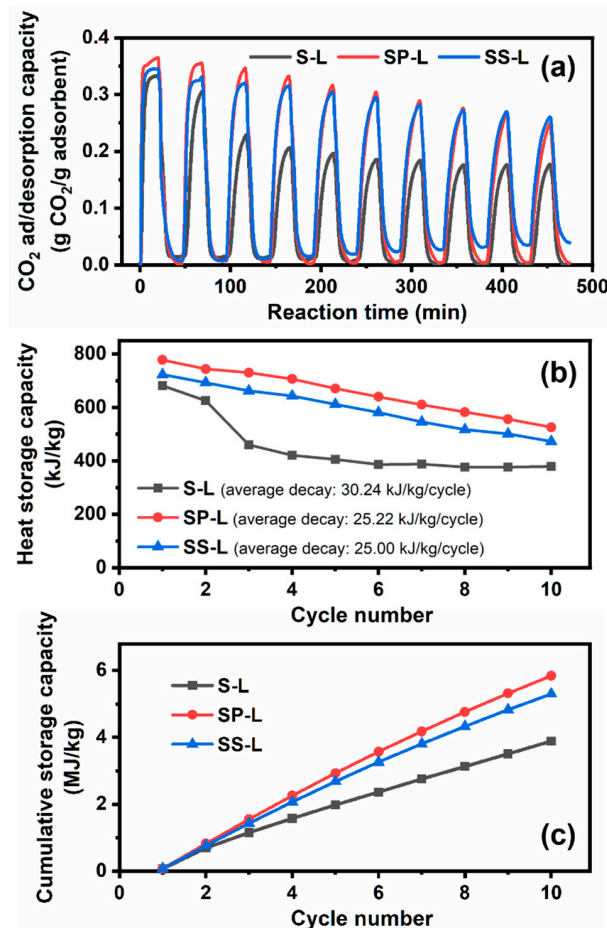


Figure 8. (a) Cyclic CO_2 ad-desorption curves, (b) heat storage capacity curves, and (c) cumulative thermochemical heat storage capacities of selected Li_4SiO_4 samples during 10 cycles.

The corresponding heat storage capacity of the samples during cyclic tests was calculated, as shown in Figure 8b. In the beginning cycle, the S-L, SP-L, and SS-L exhibited a maximum capacity of 681.7, 777.7, and 722.8 kJ/kg, which were 86.9%, 99.2%, and 92.2% of the Li_4SiO_4 's theoretical value. These relatively high conversion rates should be due to the 100% CO_2 adsorption atmosphere in Li_4SiO_4 -based TCES processes in comparison with the low CO_2 concentration (generally $<30\%$) condition used in CCS applications [39,40]. Then, as the cycle number increased, the Li_4SiO_4 samples suffered high-temperature sintering, and all of their capacities were continuously decreased at a decay rate of 25–30 kJ/kg per cycle. As a result, the capacity of the selected SP-L and SS-L declined to 525.5 and 472.7 kJ/kg at the 10th cycle, which was nearly 1.39 and 1.25 times higher than that of S-L (379.3 kJ/kg). Figure 8c further evaluates the cumulative storage capacity of samples, and there exists an obvious difference between the original S-L and the selected two samples. After 10 heat storage–releasing cycles, a cumulative amount of 5.84 and 5.30 MJ/kg was achieved for SP-L and SS-L, which were 1.39 and 1.25 times greater, respectively, than the value of S-L (3.89 MJ/kg). The heat storage performance improvements of SP-L and SS-L should be attributed to their higher purity, greater particle size, and surface morphology, as found in the former XRD, BET, SEM, and LPSA tests.

In order to find out the reason for capacity decay, the morphology of the cycled samples was observed by SEM and the $2000\times$ images, as shown in Figure 9. It is obvious that all samples turned to an agglomerate block with a much larger particle size after the cycles, which should be caused by the particle sintering during the high-temperature reactions ($720\text{ }^{\circ}\text{C}/900\text{ }^{\circ}\text{C}$). Such block structures sharply reduce the Li_4SiO_4 surface active sites and increase the CO_2 diffusion resistance during the solid–gas reaction, certainly leading to the continuous capacity decay of Li_4SiO_4 TCES materials during heat storage–releasing cycles. Especially, it has been reported that the CO_2 desorption atmosphere in this work could lead to much more severe sintering and capacity decay in comparison with commonly used moderate N_2 conditions [41,42]. Moreover, the S-L exhibited a high sintered appearance with a dense and non-porous morphology after 10 cycles, corresponding to its poor reaction performance. In comparison, the SP-L and SS-L retained a certain pore structure and showed a rough appearance with a larger surface area, resulting in the improvement of TCES performance, as has been found in former TG tests.

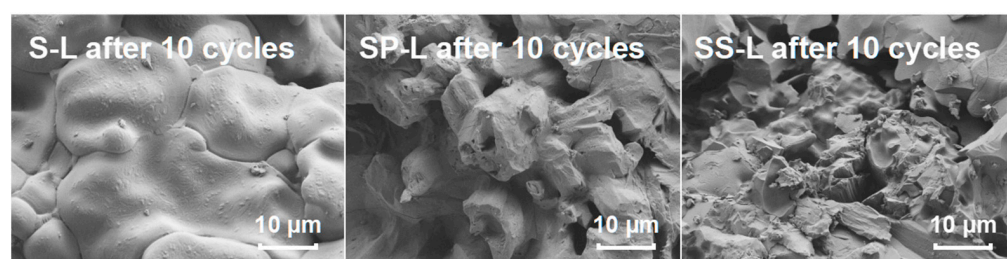


Figure 9. SEM images of S-L, SP-L, and SS-L after 10 heat storage–releasing cycles.

Finally, the multicycle heat storage capacities of Li_4SiO_4 -based TCES heat carriers reported in the literature are summarized and compared in Figure 10. As shown, in the initial cycle, the SP-L in this work possessed the highest capacity of 777.7 kJ/kg , which nearly reached the theoretical maximum value of Li_4SiO_4 . Such excellent performance should be attributed to the utilization of screened silica microspheres as Si sources, in comparison to the silica or silicon sol commonly used in other works. However, when it comes to the cyclic heat storage–releasing processes, except for the $\text{I-Li}_{3.7}\text{Fe}_{0.1}\text{SiO}_4$ and the LA-3-K, which were tested under moderate heat storage conditions (100% N_2), all reported samples more or less exhibited capacity decay due to the particle sintering during high-temperature reactions, leading to a capacity less than 600 kJ/kg after only 10 cycles. Although some attempts, such as Ce addition (L-S-Ce2.5) and K doping (L30K), have been performed to alleviate this problem to some extent, Li_4SiO_4 -based TCES heat carriers with much more stable and sintering-resistant properties should be investigated in future work for achieving the practical applications of Li_4SiO_4 - CO_2 TCES systems.

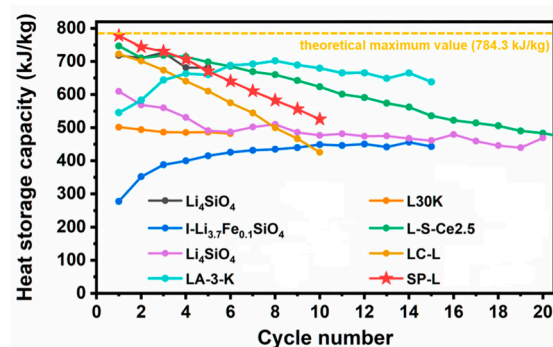


Figure 10. Comparisons of the capacities of different reported Li_4SiO_4 -based TCES materials during multiple heat storage–releasing cycles in refs. [22,28–33] and this work.

4. Conclusions

In this work, Li_4SiO_4 -based thermochemical energy storage materials were fabricated by utilizing six kinds of Si sources, including silicon dioxide, silica microspheres, silica sol, fumed silica, SBA-15, and quartz sand. The effect of different Si sources on the physicochemical properties and the TCES performance of corresponding derived Li_4SiO_4 were systematically investigated. The major conclusions are as follows:

- (1) The different kinds of Si sources varied greatly in phase compositions, morphology, and particle size. As a consequence, there were certain differences among the physicochemical properties of as-synthesized Li_4SiO_4 -based samples, especially the Li_4SiO_4 purity, thus leading to their different CO_2 capture performances as well as thermochemical energy storage performance;
- (2) Among these Li_4SiO_4 samples, those derived from silica microspheres (SPs) and silica sol (SS) exhibited the greatest and fastest isothermal CO_2 adsorption performance, as high as 0.335 g/g within only 5 min at the optimal reaction temperature (720 °C). The complete regeneration of them could also be achieved within 20 min at 900 °C;
- (3) As a result, SP-L possessed an excellent heat storage capacity as high as 777.7 kJ/kg in the initial cyclic heat storage–releasing processes. However, it suffered a capacity decay of ~25 kJ/kg/cycle due to high-temperature sintering and exhibited a cumulative heat storage amount of 5.84 MJ/kg after 10 cycles.

Author Contributions: Conceptualization, X.W.; formal analysis, X.W. and W.X. (Wentao Xia); investigation, X.W. and W.X. (Wentao Xia); writing—original draft preparation, X.W., Z.C. and Y.Y.; writing—review and editing, X.W. and Y.Y.; visualization, X.W. and W.X. (Wenlong Xu); supervision, Z.C. and Y.Y.; project administration, X.R.; funding acquisition, Y.Y. All authors have read and agreed to the published version of the manuscript.

Funding: The research was funded by the National Science Foundation of China (Grant No. 52206159) and the Youth Innovation Program of Universities in Shandong Province (Grant No. 2022KJ029).

Data Availability Statement: The original contributions presented in the study are included in the article, further inquiries can be directed to the corresponding authors.

Conflicts of Interest: The authors declare no conflict of interest.

References

1. Harindintwali, J.D.; Yuan, Z.; Wang, M.; Wang, F.; Li, S.; Yin, Z.; Huang, L.; Fu, Y.; Li, L.; Chang, S.X.; et al. Technologies and perspectives for achieving carbon neutrality. *Innovation* **2021**, *2*, 100180. [[CrossRef](#)] [[PubMed](#)]
2. Xu, M.; Yu, D.; Yao, H.; Liu, X.; Qiao, Y. Coal combustion-generated aerosols: Formation and properties. *Proc. Combust. Inst.* **2011**, *33*, 1681–1697. [[CrossRef](#)]
3. Leng, E.; Guo, Y.; Chen, J.; Liu, S.; Jiaqiang, E.; Xue, Y. A comprehensive review on lignin pyrolysis: Mechanism, modeling and the effects of inherent metals in biomass. *Fuel* **2022**, *309*, 122102. [[CrossRef](#)]
4. Wang, W.; Yuan, B.; Sun, Q.; Wennersten, R. Application of energy storage in integrated energy systems—A solution to fluctuation and uncertainty of renewable energy. *J. Energy Storage* **2022**, *52*, 104812. [[CrossRef](#)]
5. Rana, M.; Uddin, M.; Sarkar, R.; Meraj, S.T.; Shafiullah, G.; Muyeen, S.; Islam, A.; Jamal, T. Applications of energy storage systems in power grids with and without renewable energy integration—A comprehensive review. *J. Energy Storage* **2023**, *68*, 107811. [[CrossRef](#)]
6. Olabi, A. Renewable energy and energy storage systems. *Energy* **2017**, *136*, 1–6. [[CrossRef](#)]
7. Rahman, M.; Oni, A.O.; Gemechu, E.; Kumar, A. Assessment of energy storage technologies: A review. *Energy Convers. Manag.* **2020**, *223*, 113295. [[CrossRef](#)]
8. Zhang, H.; Baeyens, J.; Cáceres, G.; Degreè, J.; Lv, Y. Thermal energy storage: Recent developments and practical aspects. *Prog. Energy Combust. Sci.* **2016**, *53*, 1–40. [[CrossRef](#)]
9. Prieto, C.; Cooper, P.; Fernández, A.I.; Cabeza, L.F. Review of technology: Thermochemical energy storage for concentrated solar power plants. *Renew. Sustain. Energy Rev.* **2016**, *60*, 909–929. [[CrossRef](#)]
10. Pelay, U.; Luo, L.; Fan, Y.; Stitou, D.; Rood, M. Thermal energy storage systems for concentrated solar power plants. *Renew. Sustain. Energy Rev.* **2017**, *79*, 82–100. [[CrossRef](#)]
11. Ding, W.; Bauer, T. Progress in Research and Development of Molten Chloride Salt Technology for Next Generation Concentrated Solar Power Plants. *Engineering* **2021**, *7*, 334–347. [[CrossRef](#)]

12. Raganati, F.; Ammendola, P. Review of Carbonate-Based Systems for Thermochemical Energy Storage for Concentrating Solar Power Applications: State-of-the-Art and Outlook. *Energy Fuels* **2023**, *37*, 1777–1808. [\[CrossRef\]](#)
13. Prasad, J.S.; Muthukumar, P.; Desai, F.; Basu, D.N.; Rahman, M.M. A critical review of high-temperature reversible thermochemical energy storage systems. *Appl. Energy* **2019**, *254*, 113733. [\[CrossRef\]](#)
14. Yuan, Y.; Li, Y.; Duan, L.; Liu, H.; Zhao, J.; Wang, Z. CaO/Ca(OH)₂ thermochemical heat storage of carbide slag from calcium looping cycles for CO₂ capture. *Energy Convers. Manag.* **2018**, *174*, 8–19. [\[CrossRef\]](#)
15. Li, Y.; Song, Y.; Wu, D.; Zhang, C.; Zhu, H. Highly active and stable Ca(OH)₂-based thermochemical energy storage materials enabling direct solar absorption. *J. Energy Storage* **2024**, *84*, 110885. [\[CrossRef\]](#)
16. Zhou, Y.; Zhou, Z.; Sun, J.; Liu, L.; Luo, F.; Xu, G.; Cao, X.E.; Xu, M. Ruddlesden-Popper-type perovskite Sr₃Fe₂O₇–δ for enhanced thermochemical energy storage. *EcoMat* **2023**, *5*, e12347. [\[CrossRef\]](#)
17. Zhou, Z.; Liu, L.; Guo, Q.; Zhu, X.; Liu, X.; Xu, M. Improving the Discharge Rate of Co₃O₄-Based Thermochemical Energy Storage Material with Eutectic Doping of Zr. *Energy Fuels* **2023**, *37*, 16087–16096. [\[CrossRef\]](#)
18. Yang, L.; Huang, Z.; Huang, G. Fe- and Mn-Doped Ca-Based Materials for Thermochemical Energy Storage Systems. *Energy Fuels* **2020**, *34*, 11479–11488. [\[CrossRef\]](#)
19. Bai, S.; Sun, J.; Zhou, Z.; Bu, C.; Chen, X.; Yang, Y.; Wang, R.; Guo, Y.; Zhao, C.; Liu, W. Structurally improved, TiO₂-incorporated, CaO-based pellets for thermochemical energy storage in concentrated solar power plants. *Sol. Energy Mater. Sol. Cells* **2021**, *226*, 111076. [\[CrossRef\]](#)
20. Han, R.; Xing, S.; Wu, X.; Pang, C.; Lu, S.; Su, Y.; Liu, Q.; Song, C.; Gao, J. Relevant influence of alkali carbonate doping on the thermochemical energy storage of Ca-based natural minerals during CaO/CaCO₂ cycles. *Renew. Energy* **2021**, *181*, 267–277. [\[CrossRef\]](#)
21. Zhang, Y.; Miao, Q.; Jia, X.; Jin, Y.; Li, Z.; Tan, L.; Ding, Y. Diatomite-based magnesium sulfate composites for thermochemical energy storage: Preparation and performance investigation. *Sol. Energy* **2021**, *224*, 907–915. [\[CrossRef\]](#)
22. Takasu, H.; Ryu, J.; Kato, Y. Application of lithium orthosilicate for high-temperature thermochemical energy storage. *Appl. Energy* **2017**, *193*, 74–83. [\[CrossRef\]](#)
23. Teng, L.; Xuan, Y.; Da, Y.; Liu, X.; Ding, Y. Modified Ca-Looping materials for directly capturing solar energy and high-temperature storage. *Energy Storage Mater.* **2020**, *25*, 836–845. [\[CrossRef\]](#)
24. Zhang, Y.; Gao, Y.; Pfeiffer, H.; Louis, B.; Sun, L.; O'Hare, D.; Wang, Q. Recent advances in lithium containing ceramic based sorbents for high-temperature CO₂ capture. *J. Mater. Chem. A* **2019**, *7*, 7962–8005. [\[CrossRef\]](#)
25. Tong, Y.; Chen, S.; Huang, X.; He, Y.; Chen, J.; Qin, C. CO₂ capture by Li₂SiO₂ Sorbents: From fundamentals to applications. *Sep. Purif. Technol.* **2022**, *301*, 121977. [\[CrossRef\]](#)
26. André, L.; Abanades, S.; Flamant, G. Screening of thermochemical systems based on solid-gas reversible reactions for high temperature solar thermal energy storage. *Renew. Sustain. Energy Rev.* **2016**, *64*, 703–715. [\[CrossRef\]](#)
27. Takasu, H.; Hoshino, H.; Tamura, Y.; Kato, Y. Performance evaluation of thermochemical energy storage system based on lithium orthosilicate and zeolite. *Appl. Energy* **2019**, *240*, 1–5. [\[CrossRef\]](#)
28. Takasu, H.; Kato, Y. Reactivity enhancement of lithium orthosilicate for thermochemical energy storage material usage. *Energy Procedia* **2017**, *131*, 94–100. [\[CrossRef\]](#)
29. Fu, R.; Hu, Y.; Wang, J.; Yu, G.; Yan, S. Organolithium-derived alkali-doped highly durable Li₄SiO₄ heat carrier for solar thermochemical energy storage. *Sol. Energy Mater. Sol. Cells* **2023**, *258*, 112405. [\[CrossRef\]](#)
30. Zhang, X.; Zhou, S.; Liu, W.; Zhou, Z.; Yang, Y. Fabrication of structure-improved, sintering-resistant Li₄SiO₄ materials for stabilized thermochemical energy storage in concentrated solar power plants. *J. Energy Storage* **2023**, *70*, 108078. [\[CrossRef\]](#)
31. Fu, R.; Huang, J.; Feng, Q.; Liu, D.; Hu, Y. Synthesis of dark Li₄–₃FexSiO₄ for simultaneous direct solar thermal conversion and durable thermochemical energy storage. *J. Energy Storage* **2023**, *73*, 109053. [\[CrossRef\]](#)
32. Esaki, T.; Iwase, D.; Kobayashi, N. Evaluation of Carbon Dioxide Absorption Characteristics Lithium Ortho-Silicate in Chemical Heat Storage. *J. Mater. Sci. Chem. Eng.* **2017**, *5*, 56–63. [\[CrossRef\]](#)
33. Yan, X.; Wang, X.; Xia, W.; Lu, L.; Yang, Y.; Zhang, X.; Zhou, Z.; Liu, W. Screening of organic lithium precursors for producing high-performance Li₄SiO₄-based thermochemical energy storage materials: Experimental and kinetic investigations. *J. Energy Storage* **2024**, *85*, 111098. [\[CrossRef\]](#)
34. Seggiani, M.; Puccini, M.; Vitolo, S. Alkali promoted lithium orthosilicate for CO₂ capture at high temperature and low concentration. *Int. J. Greenh. Gas Control.* **2013**, *17*, 25–31. [\[CrossRef\]](#)
35. Yang, Y.; Chen, Z.; Sun, X.; Yao, S.; Zhang, X.; Liu, W. Li₄SiO₄ adsorbent derived from industrial biomass fly ash for high-temperature CO₂ capture. *Fuel* **2023**, *337*, 126853. [\[CrossRef\]](#)
36. Yang, Y.; Liu, W.; Hu, Y.; Sun, J.; Tong, X.; Chen, Q.; Li, Q. One-step synthesis of porous Li₄SiO₄-based adsorbent pellets via graphite moulding method for cyclic CO₂ capture. *Chem. Eng. J.* **2018**, *353*, 92–99. [\[CrossRef\]](#)
37. Yang, X.; Liu, W.; Sun, J.; Hu, Y.; Wang, W.; Chen, H.; Zhang, Y.; Li, X.; Xu, M. Preparation of Novel Li₄SiO₄ Sorbents with Superior Performance at Low CO₂ Concentration. *ChemSusChem* **2016**, *9*, 1607–1613. [\[CrossRef\]](#)
38. Izquierdo, M.T.; Turan, A.; García, S.; Maroto-Valer, M.M. Optimization of Li₄SiO₄ synthesis conditions by a solid state method for maximum CO₂ capture at high temperature. *J. Mater. Chem. A* **2018**, *6*, 3249–3257. [\[CrossRef\]](#)
39. Hu, Y.; Liu, W.; Yang, Y.; Qu, M.; Li, H. CO₂ capture by Li₄SiO₄ sorbents and their applications: Current developments and new trends. *Chem. Eng. J.* **2019**, *359*, 604–625. [\[CrossRef\]](#)

40. Lv, Z.; Ruan, J.; Tu, W.; Hu, X.; He, D.; Huang, X.; Qin, C. Integrated CO₂ capture and In-Situ methanation by efficient dual functional Li₄SiO₄@Ni/CeO₂. *Sep. Purif. Technol.* **2023**, *309*, 123044. [[CrossRef](#)]
41. Zubbri, N.A.; Mohamed, A.R.; Mohammadi, M. Parametric study and effect of calcination and carbonation conditions on the CO₂ capture performance of lithium orthosilicate sorbent. *Chin. J. Chem. Eng.* **2018**, *26*, 631–641. [[CrossRef](#)]
42. Li, H.; Qu, M.; Hu, Y. High-temperature CO₂ capture by Li₄SiO₄ adsorbents: Effects of pyroligneous acid (PA) modification and existence of CO₂ at desorption stage. *Fuel Process. Technol.* **2020**, *197*, 106186. [[CrossRef](#)]

Disclaimer/Publisher's Note: The statements, opinions and data contained in all publications are solely those of the individual author(s) and contributor(s) and not of MDPI and/or the editor(s). MDPI and/or the editor(s) disclaim responsibility for any injury to people or property resulting from any ideas, methods, instructions or products referred to in the content.